Wigner distribution measurements of the spatial coherence properties of the free-electron laser FLASH

Tobias Mey,[1,*] **Bernd Schäfer,**[1] **Klaus Mann,**[1] **Barbara Keitel,**[2]
Marion Kuhlmann,[2] **and Elke Plönjes**[2]

[1]*Laser-Laboratorium Göttingen e.V., Hans-Adolf-Krebs-Weg 1, 37077 Göttingen, Germany*
[2]*Deutsches Elektronen-Synchrotron, Notkestraße 85, 22607 Hamburg, Germany*

[*]*tobias.mey@llg-ev.de*

Abstract: The four-dimensional Wigner distribution function is determined from intensity profiles measured in the focused photon beam of FLASH (Free-electron laser in Hamburg) for a variety of photon beamline settings. The Wigner formalism results in comprehensive coherence information without the requirement of simplifying assumptions on the beam. The entire four-dimensional spatial mutual coherence function, horizontal and vertical coherence lengths and the global degree of coherence are derived and compared to Young's double pinhole measurements [Opt. Express **20**, 17480 (2012)].

References and links

1. A. Barty, S. Boutet, M. J. Bogan, S. Hau-Riege, S. Marchesini, K. Sokolowski-Tinten, N. Stojanovic, R. Tobey, H. Ehrke, A. Cavalleri, S. Düsterer, M. Frank, S. Bajt, B. W. Woods, M. Marvin Seibert, J. Hajdu, R. Treusch, and H. N. Chapman, "Ultrafast single-shot diffraction imaging of nanoscale dynamics," Nat. Photon. **2**, 415–419 (2008).
2. M. Richter, M. Y. Amusia, S. V. Bobashev, T. Feigl, P. N. Juranić, M. Martins, A. A. Sorokin, and K. Tiedtke, "Extreme ultraviolet laser excites atomic giant resonance," Phys. Rev. Lett. **102**, 163002 (2009).
3. B. Nagler, U. Zastrau, R. R. Fäustlin, S. M. Vinko, T. Whitcher, A. J. Nelson, R. Sobierajski, J. Krzywinski, J. Chalupsky, E. Abreu, S. Bajt, T. Bornath, T. Burian, H. Chapman, J. Cihelka, T. Döppner, S. Düsterer, T. Dzelzainis, M. Fajardo, E. Förster, C. Fortmann, E. Galtier, S. H. Glenzer, S. Göde, G. Gregori, V. Hajkova, P. Heimann, L. Juha, M. Jurek, F. Y. Khattak, A. R. Khorsand, D. Klinger, M. Kozlova, T. Laarmann, H. Ja Lee, R. W. Lee, K.-H. Meiwes-Broer, P. Mercere, W. J. Murphy, A. Przystawik, R. Redmer, H. Reinholz, D. Riley, G. Röpke, F. Rosmej, K. Saksl, R. Schott, R. Thiele, J. Tiggesbäumker, S. Toleikis, T. Tschentscher, I. Uschmann, H. J. Vollmer, and J. S. Wark, "Turning solid aluminium transparent by intense soft X-ray photoionization," Nat. Phys. **5**, 693–696 (2009).
4. B. Pfau, S. Schaffert, L. Müller, C. Gutt, A. Al-Shemmary, F. Büttner, R. Delaunay, S. Düsterer, S. Flewett, R. Frömter, J. Geilhufe, E. Guehrs, C. M. Günther, R. Hawaldar, M. Hille, N. Jaouen, A. Kobs, K. Li, J. Mohanty, H. Redlin, W. F. Schlotter, D. Stickler, R. Treusch, B. Vodungbo, M. Kläui, H. P. Oepen, J. Lüning, G. Grübel, and S. Eisebitt, "Ultrafast optical demagnetization manipulates nanoscale spin structure in domain walls," Nat. Commun. **3**, 1100 (2012).
5. R. N. Wilke, M. Priebe, M. Bartels, K. Giewekemeyer, A. Diaz, P. Karvinen, and T. Salditt, "Hard X-ray imaging of bacterial cells: nano-diffraction and ptychographic reconstruction," Opt. Express **20**, 19232–19254 (2012).
6. H. N. Chapman, P. Fromme, A. Barty, T. A. White, R. A. Kirian, A. Aquila, M. S. Hunter, J. Schulz, D. P. DePonte, U. Weierstall, R. B. Doak, F. R. N. C. Maia, A. V. Martin, I. Schlichting, L. Lomb, N. Coppola, R. L. Shoeman, S. W. Epp, R. Hartmann, D. Rolles, A. Rudenko, L. Foucar, N. Kimmel, G. Weidenspointner, P. Holl, M. Liang, M. Barthelmess, C. Caleman, S. Boutet, M. J. Bogan, J. Krzywinski, C. Bostedt, S. Bajt, L. Gumprecht,

B. Rudek, B. Erk, C. Schmidt, A. Hömke, C. Reich, D. Pietschner, L. Strüder, G. Hauser, H. Gorke, J. Ullrich, S. Herrmann, G. Schaller, F. Schopper, H. Soltau, K.-U. Kühnel, M. Messerschmidt, J. D. Bozek, S. P. Hau-Riege, M. Frank, C. Y. Hampton, R. G. Sierra, D. Starodub, G. J. Williams, J. Hajdu, N. Timneanu, M. M. Seibert, J. Andreasson, A. Rocker, O. Jönsson, M. Svenda, S. Stern, K. Nass, R. Andritschke, C.-D. Schröter, F. Krasniqi, M. Bott, K. E. Schmidt, X. Wang, I. Grotjohann, J. M. Holton, T. R. M. Barends, R. Neutze, S. Marchesini, R. Fromme, S. Schorb, D. Rupp, M. Adolph, T. Gorkhover, I. Andersson, H. Hirsemann, G. Potdevin, H. Graafsma, B. Nilsson, and J. C. H. Spence, "Femtosecond X-ray protein nanocrystallography," Nature **470**, 73–77 (2011).

7. M. Seibert, T. Ekeberg, F. R. N. C. Maia, M. Svenda, J. Andreasson, O. Jönsson, D. Odiè, B. Iwan, A. Rocker, D. Westphal, M. Hantke, D. P. DePonte, A. Barty, J. Schulz, L. Gumprecht, N. Coppola, A. Aquila, M. Liang, T. A. White, A. Martin, C. Caleman, S. Stern, C. Abergel, V. Seltzer, J. Claverie, C. Bostedt, J. D. Bozek, S. Boutet, A. A. Miahnahri, M. Messerschmidt, J. Krzywinski, G. Williams, K. O. Hodgson, M. J. Bogan, C. Y. Hampton, R. G. Sierra, D. Starodub, I. Andersson, S. Bajt, M. Barthelmess, J. C. H. Spence, P. Fromme, U. Weierstall, R. Kirian, M. Hunter, R. B. Doak, S. Marchesini, S. P. Hau-Riege, M. Frank, R. L. Shoeman, L. Lomb, S. W. Epp, R. Hartmann, D. Rolles, A. Rudenko, C. Schmidt, L. Foucar, N. Kimmel, P. Holl, B. Rudek, B. Erk, A. Hömke, C. Reich, D. Pietschner, G. Weidenspointner, L. Strüder, G. Hauser, H. Gorke, J. Ullrich, I. Schlichting, S. Herrmann, G. Schaller, F. Schopper, H. Soltau, K. Kühnel, R. Andritschke, C. Schröter, F. Krasniqi, M. Bott, S. Schorb, D. Rupp, M. Adolph, T. Gorkhover, H. Hirsemann, G. Potdevin, H. Graafsma, B. Nilsson, H. N. Chapman, and J. Hajdu, "Single mimivirus particles intercepted and imaged with an X-ray laser," Nature **470**, 78–81 (2011).

8. J. C. H. Spence, U. Weierstall, and M. Howells, "Coherence and sampling requirements for diffraction imaging," Ultramicroscopy **101**, 149–152 (2004).

9. L. W. Whitehead, G. J. Williams, H. M. Quiney, D. J. Vine, R. A. Dilanian, S. Flewett, K. A. Nugent, A. G. Peele, E. Balaur, and I. McNulty, "Diffractive imaging using partially coherent X rays," Phys. Rev. Lett. **103**, 243902 (2009).

10. B. Chen, B. Abbey, R. Dilanian, E. Balaur, G. van Riessen, M. Junker, C. Q. Tran, M. W. M. Jones, A. G. Peele, I. McNulty, D. J. Vine, C. T. Putkunz, H. M. Quiney, and K. A. Nugent, "Diffraction imaging: The limits of partial coherence," Phys. Rev. B **86**, 235401 (2012).

11. M. Born and E. Wolf, *Principles of Optics* (Cambridge University, 1980).

12. R. Ischebeck, J. Feldhaus, C. Gerth, E. Saldin, P. Schmüser, E. Schneidmiller, B. Steeg, K. Tiedtke, M. Tonutti, R Treusch, and M Yurkov, "Study of the transverse coherence at the TTF free electron laser," Nucl. Instrum. Methods A **507**, 175–180 (2003).

13. I. A. Vartanyants, A. Singer, A. P. Mancuso, O. M. Yefanov, A. Sakdinawat, Y. Liu, E. Bang, G. J. Williams, G. Cadenazzi, B. Abbey, H. Sinn, D. Attwood, K. A. Nugent, E. Weckert, T. Wang, D. Zhu, B. Wu, C. Graves, A. Scherz, J. J. Turner, W. F. Schlotter, M. Messerschmidt, J. Lüning, Y. Acremann, P. Heimann, D. C. Mancini, V. Joshi, J. Krzywinski, R. Soufli, M. Fernandez-Perea, S. Hau-Riege, A. G. Peele, Y. Feng, O. Krupin, S. Moeller, and W. Wurth, "Coherence properties of individual femtosecond pulses of an X-ray free-electron laser," Phys. Rev. Lett. **107**, 144801 (2011).

14. A. Singer, F. Sorgenfrei, A. P. Mancuso, N. Gerasimova, O. M. Yefanov, J. Gulden, T. Gorniak, T. Senkbeil, A. Sakdinawat, Y. Liu, D. Attwood, S. Dziarzhytski, D. D. Mai, R. Treusch, E. Weckert, T. Salditt, A. Rosenhahn, W. Wurth, and I. A. Vartanyants, "Spatial and temporal coherence properties of single free-electron laser pulses," Opt. Express **20**, 17480–17495 (2012).

15. F. Capotondi, E. Pedersoli, N. Mahne, R. H. Menk, G. Passos, L. Raimondi, C. Svetina, G. Sandrin, M. Zangrando, M. Kiskinova, S. Bajt, M. Barthelmess, H. Fleckenstein, H. N. Chapman, J. Schulz, J. Bach, R. Frömter, S. Schleitzer, L. Müller, C. Gutt, and G. Grübel, "Coherent imaging using seeded free-electron laser pulses with variable polarization: First results and research opportunities," Rev. Sci. Instrum. **84**, 051301 (2013).

16. M. J. Bastiaans, "The Wigner distribution function applied to optical signals and systems," Opt. Commun. **25**, 26–30 (1978).

17. M. J. Bastiaans, "The Wigner distribution function and its application to first-order optics," J. Opt. Soc. Am. **69**, 1710–1716 (1979).

18. M. J. Bastiaans, "Application of the Wigner distribution function to partially coherent light," J. Opt. Soc. Am. A **3**, 1227–1238 (1986).

19. B. Eppich and N. Reng, "Measurement of the Wigner distribution function based on the inverse Radontransformation," Proc. SPIE **2375**, 261–268 (1995).

20. B. Eppich, S. Johansson, H. Laabs, and H. Weber, "Measuring laser beam parameters: phase and spatial coherence using the Wigner function," Proc. SPIE **3930**, 76–86 (2000).

21. A. Cámara, T. Alieva, J. A. Rodrigo, and M. L. Calvo, "Tomographic reconstruction of the Wigner distribution of non-separable beams," in *PIERS Cambridge* (2010).

22. B. Schäfer and K. Mann, "Characterization of an ArF excimer laser beam from measurements of the Wigner distribution function," New J. Phys. **13**, 043013 (2011).

23. C. Q. Tran, G. J. Williams, A. Roberts, S. Flewett, A. G. Peele, D. Paterson, M. D. de Jonge, and K. A. Nugent, "Experimental measurement of the four-dimensional coherence function for an undulator X-ray source," Phys. Rev. Lett. **98**, 224801 (2007).

24. B. Schäfer, B. Flöter, T. Mey, P. Juranic, S. Kapitzki, B. Keitel, E. Plönjes, K. Mann, and K. Tiedtke, "FEL beam characterization from measurements of the Wigner distribution function," Nucl. Instrum. Methods A **654**, 502–507 (2011).

25. P. Toft, "The Radon transform - theory and implementation," PhD Thesis, Department of Mathematical Modelling, Technical University of Denmark (1996).

26. B. Eppich, "Die Charakterisierung von Strahlungsfeldern mit der Wigner-Verteilung und deren Messung," PhD Thesis, Technische Universität Berlin (1998).

27. R. Castaneda and F. F. Medina, "On spatial coherence beams," Optik **109**, 77–83 (1998).

28. W. Ackermann, G. Asova, V. Ayvazyan, A. Azima, N. Baboi, J. Bähr, V. Balandin, B. Beutner, A. Brandt, A. Bolzmann, R. Brinkmann, O. I. Brovko, M. Castellano, P. Castro, L. Catani, E. Chiadroni, S. Choroba, A. Cianchi, J. T. Costello, D. Cubaynes, J. Dardis, W. Decking, H. Delsim-Hashemi, A. Delserieys, G. Di Pirro, M. Dohlus, S. Düsterer, A. Eckhardt, H. T. Edwards, B. Faatz, J. Feldhaus, K. Flöttmann, J. Frisch, L. Fröhlich, T. Garvey, U. Gensch, Ch. Gerth, M. Görler, N. Golubeva, H.-J. Grabosch, M. Grecki, O. Grimm, K. Hacker, U. Hahn, J. H. Han, K. Honkavaara, T. Hott, M. Hüning, Y. Ivanisenko, E. Jaeschke, W. Jalmuzna, T. Jezynski, R. Kammering, V. Katalev, K. Kavanagh, E. T. Kennedy, S. Khodyachykh, K. Klose, V. Kocharyan, M. Körfer, M. Kollewe, W. Koprek, S. Korepanov, D. Kostin, M. Krassilnikov, G. Kube, M. Kuhlmann, C. L. S. Lewis, L. Lilje, T. Limberg, D. Lipka, F. Löhl, H. Luna, M. Luong, M. Martins, M. Meyer, P. Michelato, V. Miltchev, W. D. Möller, L. Monaco, W. F. O. Müller, O. Napieralski, O. Napoly, P. Nicolosi, D. Nülle, T. Nuñez, A. Oppelt, C. Pagani, R. Paparella, N. Pchalek, J. Pedregosa-Gutierrez, B. Petersen, B. Petrosyan, G. Petrosyan, L. Petrosyan, J. Pflüger, E. Plönjes, L. Poletto, K. Pozniak, E. Prat, D. Proch, P. Pucyk, P. Radcliffe, H. Redlin, K. Rehlich, M. Richter, M. Roehrs, J. Roensch, R. Romaniuk, M. Ross, J. Rossbach, V.Rybnikov, M. Sachwitz, E. L. Saldin, W. Sandner, H. Schlarb, B. Schmidt, M. Schmitz, P. Schmüser, J. R. Schneider, E. A. Schneidmiller, S. Schnepp, S. Schreiber, M. Seidel, D. Sertore, A. V. Shabunov, C. Simon, S. Simrock, E. Sombrowski, A. A. Sorokin, P. Spanknebel, R. Spesyvtsev, L. Staykov, B. Steffen, F. Stephan, F. Stulle, H. Thom, K. Tiedtke, M. Tischer, S. Toleikis, R. Treusch, D. Trines, I. Tsakov, E. Vogel, T. Weiland, H. Weise, M. Wellhöfer, M. Wendt, I. Will, A. Winter, K. Wittenburg, W. Wurth, P. Yeates, M. V. Yurkov, I. Zagorodnov, and K. Zapfe, "Operation of a free-electron laser from the extreme ultraviolet to the water window," Nat. Photonics **1**, 336–342 (2007).

29. V. Ayvazyan, N. Baboi, J. Bähr, V. Balandin, B. Beutner, A. Brandt, I. Bohnet, A. Bolzmann, R. Brinkmann, O. I. Brovko, J. P. Carneiro, S. Casalbuoni, M. Castellano, P. Castro, L. Catani, E. Chiadroni, S. Choroba, A. Cianchi, H. Delsim-Hashemi, G. Di Pirro, M. Dohlus, S. Düsterer, H. T. Edwards, B. Faatz, A. A. Fateev, J. Feldhaus, K. Flöttmann, J. Frisch, L. Fröhlich, T. Garvey, U. Gensch, N. Golubeva, H.-J. Grabosch, B. Grigoryan, O. Grimm, U. Hahn, J. H. Han, M. V. Hartrott, K. Honkavaara, M. Hüning, R. Ischebeck, E. Jaeschke, M. Jablonka, R. Kammering, V. Katalev, B. Keitel, S. Khodyachykh, Y. Kim, V. Kocharyan, M. Körfer, M. Kollewe, D. Kostin, D. Krämer, M. Krassilnikov, G. Kube, L. Lilje, T. Limberg, D. Lipka, F. Löhl, M. Luong, C. Magne, J. Menzel, P. Michelato, V. Miltchev, M. Minty, W. D. Möller, L. Monaco, W. Müller, M. Nagl, O. Napoly, P. Nicolosi, D. Nölle, T. Nuñez, A. Oppelt, C. Pagani, R. Paparella, B. Petersen, B. Petrosyan, J. Pflüger, P. Piot, E. Plönjes, L. Poletto, D. Proch, D. Pugachov, K. Rehlich, D. Richter, S. Riemann, M. Ross, J. Rossbach, M. Sachwitz, E. L. Saldin, W. Sandner, H. Schlarb, B. Schmidt, M. Schmitz, P. Schmüser, J. R. Schneider, E. A. Schneidmiller, H.-J. Schreiber, S. Schreiber, A. V. Shabunov, D. Sertore, S. Setzer, S. Simrock, E. Sombrowski, L. Staykov, B. Steffen, F. Stephan, F. Stulle, K. P. Sytchev, H. Thom, K. Tiedtke, M. Tischer, R. Treusch, D. Trines, I. Tsakov, A. Vardanyan, R. Wanzenberg, T. Weiland, H. Weise, M. Wendt, I. Will, A. Winter, K. Wittenburg, M. V. Yurkov, I. Zagorodnov, P. Zambolin, and K. Zapfe, "First operation of a free-electron laser generating GW power radiation at 32 nm wavelength," Eur. Phys. J. D **37**, 297–303 (2006).

30. S. Schreiber, "First lasing in the water window with 4.1 nm at FLASH," in Proc. FEL2011 (Shanghai) (2011), pp. 164–165.

31. K. Tiedtke, A. Azima, N. von Bargen, L. Bittner, S. Bonfigt, S. Düsterer, B. Faatz, U. Frühling, M. Gensch, C. Gerth, N. Guerassimova, U. Hahn, T. Hans, M. Hesse, K. Honkavaar, U. Jastrow, P. Juranic, S. Kapitzki, B. Keitel, T. Kracht, M. Kuhlmann, W. B. Li, M. Martins, T. Nuñez, E. Plönjes, H. Redlin, E. L. Saldin, E. A. Schneidmiller, J. R. Schneider, S. Schreiber, N. Stojanovic, F. Tavella, S. Toleikis, R. Treusch, H. Weigelt, M. Wellhöfer, H. Wabnitz, M. V. Yurkov, and J. Feldhaus, "The soft x-ray free-electron laser FLASH at DESY: beamlines, diagnostics and end-stations," New J. Phys. **11**, 023029 (2009).

32. S. Düsterer, P. Radcliffe, G. Geloni, U. Jastrow, M. Kuhlmann, E. Plönjes, K. Tiedtke, R. Treusch, J. Feldhaus, P. Nicolosi, L. Poletto, P. Yeates, H. Luna, J. T. Costello, P. Orr, D. Cubaynes, and M. Meyer, "Spectroscopic characterization of vacuum ultraviolet free electron laser pulses," Opt. Lett. **31**, 1750–1752 (2006).

33. B. L. Henke, E. M. Gullikson, and J. C. Davis, "X-ray interactions: photoabsorption, scattering, transmission, and reflection at E=50-30000 eV, Z=1-92," At. Data. Nucl. Data Tables **54**, 181–342 (1993).

34. ISO/DIS 11146-1, Lasers and laser-related equipment - Test methods for laser beam widths, divergence angle and beam propagation ratio (2005).

35. F. Siewert, J. Buchheim, T. Zeschke, G. Brenner, S. Kapitzki, and K. Tiedtke, "Sub-nm accuracy metrology for ultra-precise reflective X-ray optics," Nucl. Instrum. Methods A **635**, S52–S57 (2011).

36. L. Mandel and E. Wolf, *Optical Coherence and Quantum Optics* (Cambridge University, 1995).

37. B. Flöter, P. Juranić, S. Kapitzki, B. Keitel, K. Mann, E. Plönjes, B. Schäfer, and K. Tiedtke, "EUV Hartmann

sensor for wavefront measurements at the Free-electron LASer in Hamburg," New J. Phys. **12**, 083015 (2010).
38. A. Singer and I. A. Vartanyants, "Modelling of partially coherent radiation based on the coherent mode decomposition," Proc. SPIE **8141**, 814106 (2011).

1. Introduction

Free-Electron Lasers (FELs) can emit highly coherent and extremely brilliant radiation in the soft and hard x-ray regime with pulse lengths in the fs range. In the past years, these sources have opened new research opportunities in a many fields [1–4]. In particular, coherent diffractive imaging (CDI) of biological cells, proteins or viruses [5–7] now opens up a broad new field of research in life sciences. This imaging technique strongly depends on a high flux of fully coherent photons. In conventional CDI, the coherence length of the illuminating beam needs to be at least twice as large as the lateral extent of the investigated object [8]. However, CDI results could successfully be achieved even with less coherent beams applying newly developed algorithms which take partial coherence into account [9, 10]. Yet, a comprehensive knowledge of the coherence properties of the employed beam is essential.

A standard approach to gain information on the coherence properties of a radiation field is Young's double pinhole experiment [11] which has been previously applied to both SASE (self-amplification of spontaneous emission) [12–14] and seeded [15] FEL beam sources. For single pulses the local degree of coherence between two points in the beam is deduced from the interference pattern generated by the two pinholes. Assuming a Gaussian Shell-model beam, it is possible to determine the coherence length of the beam and the global degree of coherence K by using various pinhole separations. However, in order to provide the entire four-dimensional mutual coherence function $\Gamma(\vec{x}, \vec{s})$ with an adequate resolution hundreds of thousands of separate measurements are required.

As an alternative technique to determine $\Gamma(\vec{x}, \vec{s})$ with acceptable effort, we use the formalism of the Wigner distribution function (WDF) $h(\vec{x}, \vec{s})$, which is the two-dimensional Fourier transform of the mutual coherence function [16–18]. $h(\vec{x}, \vec{s})$ can be determined by measuring a reasonable number of intensity profiles at various positions in the caustic of the FEL beam behind a focusing optic. Subsequently, a Fourier back-transform yields $\Gamma(\vec{x}, \vec{s})$, and the coherence lengths as well as the global degree of coherence can be deduced.

This method is well known from studies with visible and excimer lasers [19–22]. It has also been applied to synchrotron and FEL sources [23, 24], but only under the assumption of separable beams, i.e. the intensity distribution $I(x,y)$ can be always written as a product $I(x) \cdot I(y)$. This property applies to simple beam structures such as a Gaussian Shell-model beam, but it cannot be assigned to complex radiation fields. Here, we extend the formalism to include non-separable beams and apply it to the photon beam of FLASH under various experimental conditions. These results are compared to the existing studies employing Young's double pinhole experiment [14].

2. Theory

The Wigner distribution $h(\vec{x}, \vec{u})$ of a quasi-monochromatic paraxial beam is defined in terms of a two-dimensional Fourier transform of the mutual coherence function Γ [16, 18]

$$h(\vec{x}, \vec{u}) = \left(\frac{k}{2\pi}\right)^2 \int \Gamma(\vec{x}, \vec{s}) \, e^{ik\vec{u}\cdot\vec{s}} d^2s \tag{1}$$

where $\vec{x} = (x, y)$ and $\vec{s} = (s_x, s_y)$ are two-dimensional spatial and $\vec{u} = (u, v)$ angular coordinates in a plane perpendicular to the direction of beam propagation and k is the mean wave number.

The marginal distributions of $h(\vec{x}, \vec{u})$ with respect to $\vec{x}$ and $\vec{u}$ are always non-negative and yield the irradiance (near field) $I(\vec{x})$ and the radiant intensity (far field) $I_{\mathrm{ff}}(\vec{u})$, respectively.

The propagation of the Wigner distribution is discussed elsewhere [24] and results in the projection slice theorem of tomography [25]

$$\tilde{h}_{\mathrm{ref}}\left(\vec{w}, \frac{z}{z_R} \cdot \vec{w}\right) = \tilde{I}_z(\vec{w}),$$

(2)

which states that each Fourier transformed intensity distribution $\tilde{I}_z(\vec{w})$ at position z represents a two-dimensional plane with the slope $\frac{z}{z_R}$ and the corresponding angle $\phi = \arctan\left(\frac{z}{z_R}\right)$ in the four-dimensional reciprocal phase space (z_R denotes the mean Rayleigh length, $\vec{w} = (w_x, w_y)$ the reciprocal spatial coordinate).

When $h(\vec{x}, \vec{u})$ is known, the centered second order beam moments can be computed by [17]

$$\langle x^2 \rangle = \frac{\int (x - \langle x \rangle)^2 \cdot h(\vec{x}, \vec{u}) \, d\vec{x} d\vec{u}}{\int h(\vec{x}, \vec{u}) \, d\vec{x} d\vec{u}}$$

(3)

(correspondingly for $\langle xu \rangle$, $\langle u^2 \rangle$, etc.) from which the following beam propagation parameters can be deduced [26]

- ○ beam diameter $d_x = 4\sqrt{\langle x^2 \rangle}$

- ○ waist diameter $d_{0,x} = 4\sqrt{\langle x^2 \rangle - \frac{\langle xu \rangle^2}{\langle u^2 \rangle}}$

- ○ beam divergence $\theta_u = 4\sqrt{\langle u^2 \rangle}$

- ○ beam quality factor $M_x^2 = 2k\sqrt{\langle x^2 \rangle \langle u^2 \rangle - \langle xu \rangle^2}$

Analogue relations hold for the corresponding vertical parameters.

The mutual coherence function Γ is related to the Wigner distribution through a two-dimensional Fourier back-transform

$$\Gamma(\vec{x}, \vec{s}) = \int h(\vec{x}, \vec{u}) \, e^{-ik\vec{u}\cdot\vec{s}} d^2 u$$

(4)

from which the lateral coherence length l_x (and correspondingly l_y) is derived by [27]

$$l_x = \sqrt{8 \frac{\int (s_x - \langle s_x \rangle)^2 \, |\Gamma(\vec{x}, \vec{s})|^2 \, d^2x d^2s}{\int |\Gamma(\vec{x}, \vec{s})|^2 \, d^2x d^2s}}.$$

(5)

The local degree of coherence is related to Γ through

$$\gamma(\vec{x}, \vec{s}) = \frac{\Gamma(\vec{x}, \vec{s})}{\sqrt{\Gamma(\vec{x} - \vec{s}/2, 0) \cdot \Gamma(\vec{x} + \vec{s}/2, 0)}}.$$

(6)

Finally, the global degree of coherence K is given by

$$K = \frac{\lambda^2}{P^2} \int h(\vec{x}, \vec{u})^2 \, d^2x d^2u$$

(7)

with the wavelength λ and the total power of the beam $P = \int h(\vec{x}, \vec{u}) \, d^2x d^2u$.

3. Experimental

FLASH is a single-pass free electron laser based on the SASE (self-amplification of spontaneous emission) process. It provides highly intense, short-pulsed radiation in the wavelength range from $47 - 4.2\,$nm [28–30]. Since the exponential amplification process in a SASE FEL starts from shot noise generated by the electron bunch, the photon radiation itself is of stochastic nature and individual radiation pulses differ in their intensity, temporal structure, and spectral distribution.

The measurements have been performed at beamlines BL2 and BL3 of FLASH with the FEL operating in single pulse mode at 10 Hz repetition rate. The bunch charge of the electron beam was set to values between $0.44 - 0.54\,$nC and the soft x-ray photon beam was generated with intensities in the range of $30 - 50\,\mu$J. Two circular apertures are positioned in the photon beam $18.8\,$m and $23.3\,$m behind the center of the last undulator, i.e. the expected source position, to be able to confine the beam size. During the experiments always two apertures of equal size were used, available diameters are $10\,$mm, $5\,$mm, $3\,$mm and $1\,$mm. A general description of the FLASH user facility can be found in [31].
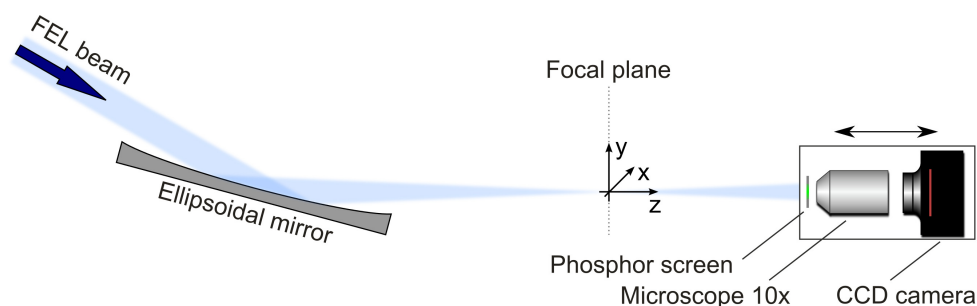
Fig. 1. Scheme of the experimental setup.

In our first measurement campaign at beamline BL3, the FLASH beam was tuned to a fundamental wavelength of $24.7\,$nm. The beam was attenuated by two filters, a $200\,$nm thick, meshless Zr filter and a $198\,$nm thick, meshless Al filter, to prevent saturation of the phosphor screen in the experimental setup, shown in Fig. 1 and described below. Thus, based on previous studies on the spectral composition of the FLASH beam [28, 32] and the theoretical filter transmissions [33], we attribute 80% of the beam energy to the fundamental wavelength, 18% to the third harmonic and 2% to the fifth harmonic. Since the fundamental dominates for this attenuation scheme, we treat the beam as monochromatic at $\lambda = 24.7\,$nm. During the measurements at BL2 ($\lambda = 25.8\,$nm) a $101\,$nm thick Al filter together with a $420\,$nm thick Si filter were used, both self-supporting. This filter combination leads to a strong suppression of the higher harmonics and nearly 100% of the transmitted beam energy is concentrated in the fundamental wavelength.

The experimental setup is shown schematically in Fig. 1. At both beamlines BL2 and BL3, the incoming FEL beam is focused by the ellipsoidal beamline mirror producing a focal spot $2\,$m behind the center of the mirror [31]. In our experimental setup a phosphorous screen, which is movable under vacuum, intercepts the beam in various positions along the caustic. Thus, the beam profiles are converted into visible wavelengths by the screen which has a grain size of $1\,\mu$m and a thickness of $4\,\mu$m. The screen is imaged by a 10x magnifying objective to a CCD camera with 1280 x 1024 pixels, each $6.45\,\mu$m in size and with a dynamic range of 12bit. Since single pulse exposures lead to saturation effects of the phosphor screen the exposure time is

$1500 - 1800$ ms comprising between 15 and 18 pulses depending on the attenuation scheme for the corresponding measurement. A motorized translation stage allows for an automated movement of the detector in beam direction which covers a range of up to ± 11 Rayleigh lengths around the beam waist. An entire measurement involves 145 different positions z_i being distributed as

$$z_i = z_R \tan \phi_i \qquad (8)$$

with the mean Rayleigh length z_R and equidistant angles ϕ_i. This represents tight sampling close to beam waist becoming coarser further out. For the reconstruction of the Wigner distribution this results in a uniform mapping of the phase space.

4. Evaluation

Data evaluation starts with a background correction of the obtained intensity distributions by subtraction of a dark image and a small offset to eliminate noise effects. Then, via the second order moments method [34], intensity profiles are centered and Rayleigh length z_R and waist position z_0 are derived in terms of mean values for x- and y-direction, i.e. $z_R = 1/2 \cdot (z_{R,x} + z_{R,y})$. In the following the mean waist position z_0 is chosen as the origin of the z-axis.

Reconstruction of the Wigner distribution is done on a four-dimensional regular grid containing 129^4 cells. Following Eq. (2) the Fourier space of h is filled with data from intensity profiles measured at different positions z_i. If more than one value contributes to a single cell, the arithmetic average is applied. For cells which remain empty after the mapping, an interpolation is being computed by the mean value of those adjacent cells which are non-zero. Finally, a four-dimensional Fourier back-transform of $\tilde{h}$ results the Wigner distribution function $h(\vec{x}, \vec{u})$.

All beam parameters presented in this study are derived from the reconstructed Wigner distribution function as described in section 2.

5. Results

First, we discuss the measurement at a wavelength of $\lambda = 24.7$ nm with two 10 mm apertures in the beamline. After a discussion of the accuracy of the applied algorithm we investigate the influence of smaller apertures on the beam properties.

(a) $z = -44$ mm   (b) $z = 0$ mm   (c) $z = 97$ mm
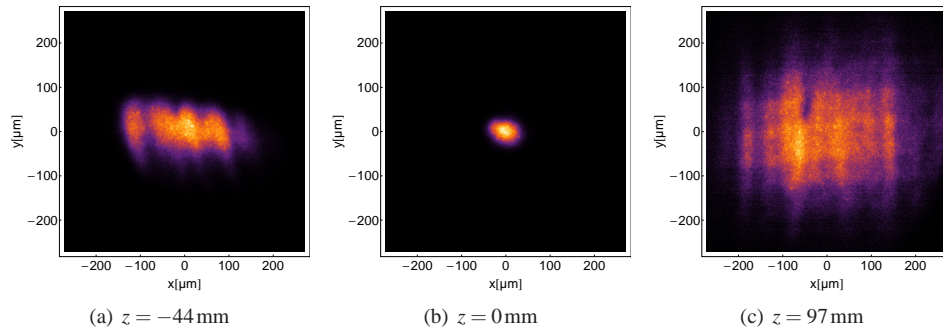
Fig. 2. Normalized intensity profiles of the FLASH beam measured at distinct positions ($\lambda = 24.7$ nm, 10 mm diameter apertures).

As an example, three intensity profiles captured at various positions are shown in Fig. 2. While close to the focal position, i.e. $z = 0$, the beam profile appears uniformly distributed,

a modulation in *x*-direction develops for increasing distances. We assume that this can be attributed to small imperfections of the surface of the ellipsoidal mirror which would affect especially the horizontal propagation characteristics due to the orientation of its long axis (see Fig. 1) as it is under present investigation [35].

(a) $h_x(x,u) = \int h(\vec{x},\vec{u})\, dy\, dv$ (b) $h_y(y,v) = \int h(\vec{x},\vec{u})\, dx\, du$
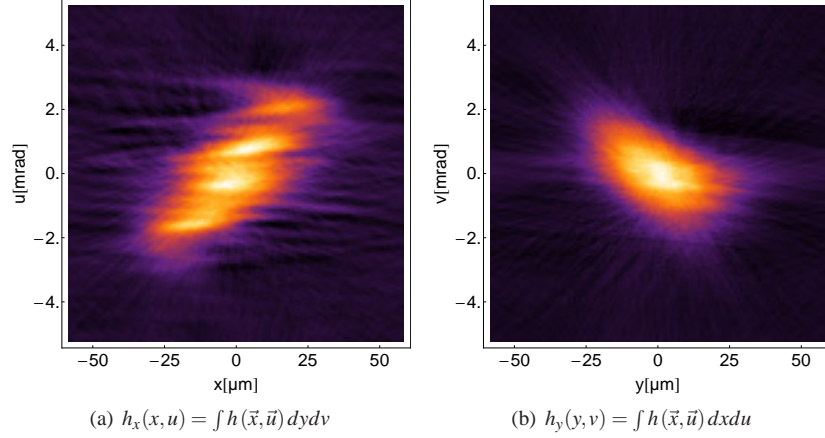
Fig. 3. Projections of the Wigner distribution function of the FLASH beam ($\lambda = 24.7\,\text{nm}$, 10 mm diameter apertures).

The Wigner distribution function $h(\vec{x},\vec{u})$, reconstructed from 145 intensity profiles as described in section 4, is shown in terms of projections $h_x(x,u)$ and $h_y(y,v)$ in Fig. 3. This way, the properties of beam propagation are resembled separately for horizontal and vertical direction. Apparently, while $h_x(x,u)$ is distributed smoothly in spatial direction x, it shows a stripe structure in angular direction u. This is caused by the uniform near field profile and the developing horizontal intensity modulation when approaching the far field. In contrast, $h_y(y,v)$ is distributed rather Gaussian like for both axes y and v corresponding to the vertical properties of the intensity profiles in near and far field.

h is real, since the value of $P = \int h(\vec{x},\vec{u}) d^2x\, d^2u$ reveals a real part on the order of 1 and an imaginary part on the order of 10^{-18}. Hence, the derived mutual coherence function follows hermitian symmetry.

From the Wigner distribution, we compute beam divergences $\theta_u = 5.2\,\text{mrad}$ and $\theta_v = 3.6\,\text{mrad}$, waist diameters $d_{0,x} = 52\,\mu\text{m}$ and $d_{0,y} = 41\,\mu\text{m}$ and beam quality factors $M_x^2 = 8.6$ and $M_y^2 = 4.6$. While θ quantifies the extent of h in the respective angular direction, d_0 gives the spatial extent of h when propagated to corresponding waist positions, i.e. where $\langle xu \rangle$ or $\langle yv \rangle$ vanish. The positions of the foci are found at $z_{0,x} = 8.88\,\text{mm}$ and $z_{0,y} = -8.88\,\text{mm}$, revealing an astigmatic aberration.

The resulting mutual coherence function is given in terms of sections $|\Gamma_x(x,s_x)|$ and $|\Gamma_y(y,s_y)|$ in Fig. 4. While for $s_x = 0$ and $s_y = 0$ these distributions represent the intensity $I(x,0)$ and $I(0,y)$ at mean waist position z_0, for increasing s_x and s_y the decay of the coherence is revealed. Equation (5) is employed to quantify the coherence lengths l_x and l_y. The values are always given in spatial units and as a fraction of the beam diameters d_x and d_y at mean waist position, which can be larger than the waist diameters $d_{0,x}$ and $d_{0,y}$. For the FLASH beam we find $l_x = 9.0\,\mu\text{m}$ and $l_y = 11.6\,\mu\text{m}$, representing a fraction of 0.13 and 0.22 of the horizontal and vertical beam diameter, respectively.

The local degree of coherence is depicted in Fig. 5 in terms of the sections $|\gamma_x(s_x)| = |\gamma(0,0,s_x,0)|$ and $|\gamma_y(s_y)| = |\gamma(0,0,0,s_y)|$ and can be directly compared to results derived by

(a) $|\Gamma_x(x,s_x)| = |\Gamma(x,0,s_x,0)|$ (b) $|\Gamma_y(y,s_y)| = |\Gamma(0,y,0,s_y)|$
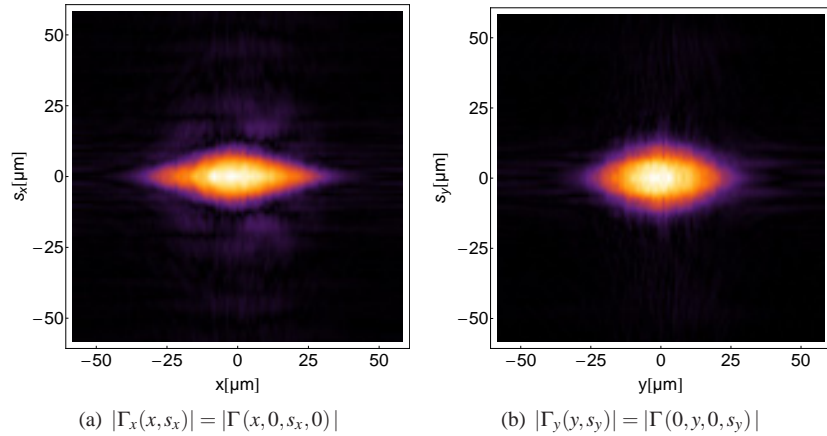
Fig. 4. Sections of the mutual coherence function of the FLASH beam represented by absolute values ($\lambda = 24.7\,\text{nm}$, $10\,\text{mm}$ diameter apertures).

Singer *et al* with Young's experiment [14]. Evaluating the variance of the Gaussian fit functions $\exp\left(-s^2/(2\sigma^2)\right)$ yields $\sigma_x = 5.5\,\mu\text{m}$ and $\sigma_y = 7.2\,\mu\text{m}$, which is only slightly below the values of reference [14] which gives $6.2 \pm 0.9\,\mu\text{m}$ and $8.7 \pm 1.0\,\mu\text{m}$ for horizontal and vertical direction, respectively.
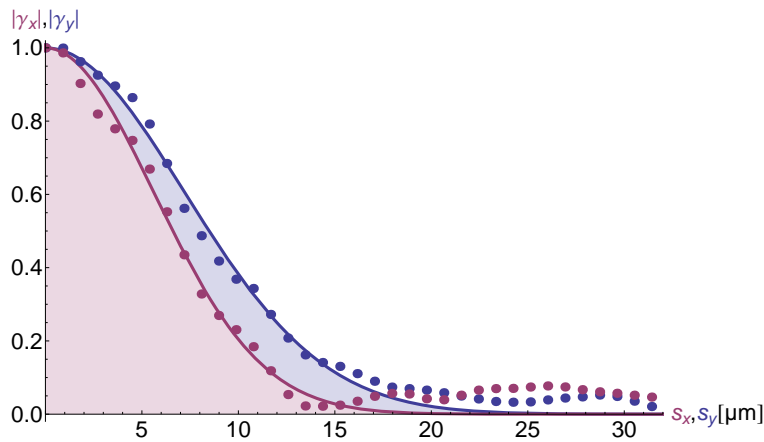
Fig. 5. Sections $|\gamma_x(s_x)| = |\gamma(0,0,s_x,0)|$ and $|\gamma_y(s_y)| = |\gamma(0,0,0,s_y)|$ of the local degree of coherence ($\lambda = 24.7\,\text{nm}$, $10\,\text{mm}$ diameter apertures).

Assuming a Gaussian Shell-model beam [36], the following relation holds between the coherence length l, the variance σ of γ and the beam diameter d

$$\frac{1}{l^2} = \frac{1}{4\sigma^2} + \frac{1}{d^2}.$$

(9)

Thus, we can derive coherence lengths from the values of Singer *et al* being comparable to our values for l, cf. Table 1. Again, we find a good agreement between both techniques. However, it should be noted that our values for the beam diameter are significantly larger than those obtained by PMMA imprints at a wavelength of 8.0 nm by Singer *et al*. A summary is given in Table 1.

Table 1. Comparison between results from measurement of the Wigner distribution and from Young's double pinhole experiment [14]: Variance σ of $|\gamma(\vec{s})|$, coherence length l and beam diameter d. (Young's experiment: $\lambda = 8.0$ nm, Wigner formalism: $\lambda = 24.7$ nm, in both cases 10 mm diameter apertures are employed)

	Wigner formalism			Young's experiment		
	$\sigma[\mu m]$	$l[\mu m]$	$d[\mu m]$	$\sigma[\mu m]$	$l[\mu m]$	$d[\mu m]$
horizontal direction	5.5	9.0	67	6.2	10.0	17
vertical direction	7.2	11.6	53	8.7	12.2	17

Finally, employing Eq. (7) the global degree of coherence is $K = 0.032$. In comparison, $K = 0.42 \pm 0.09$ derived from Young's double pinhole experiment at $\lambda = 8.0$ nm is significantly higher [14]. This can be attributed to the strongly different beam diameters in both measurements. At the three times shorter wavelength of 8.0 nm for Young's experiment compared to 24.7 nm in our case a significantly smaller beam diameter is to be expected. On the one hand, the multi pulse exposure in our experiment might lead to an overestimation due to a pointing instability, one the other hand, the evaluation of PMMA imprints can also result in underestimated beam sizes [37]. Since the relation $K_{GS} = \frac{l_x}{d_x}\frac{l_y}{d_y}$ holds for a Gaussian Shell-model beam [36], the global degree of coherence is strongly dependent on the derived beam diameters. Within the limits of this simplification and with our values for $d_{x,y}$ and $l_{x,y}$ $K_{GS} = 0.029$ is calculated which is close to the value obtained by Eq. (7). Hence, only the central fraction of the beam can be regarded as coherent and it can be approximated by an ellipse with the half-axes l_x and l_y. This is illustrated in Fig. 6 which shows the reconstruction of the intensity distribution at $z = 0$ according to $I(\vec{x}) = \int h(\vec{x}, \vec{u}) d^2 u$ together with the measured beam profile. Additionally, the coherent fraction of the beam is indicated by ellipses which are spanned by the coherence lengths and the beam diameters.

Here, it should be clarified that the applied formalism which reconstructs the Wigner distribution characterizes a large ensemble of individual pulses. Thus, pulse-to-pulse fluctuations in the coherence properties, as expected due to the statistical SASE process, are averaged to *mean* values. During Young's experiment, for a certain pinhole distance, many different values for the local degree of coherence have been measured for individual pulses. These fluctuations could be due to a pointing instability but could also well be attributed to inherent coherence fluctuations. However, in the Singer experiment only the most coherent pulses have been employed for evaluation which results in the *best* coherence properties that can be expected for the FLASH beam.

5.1. Accuracy estimation

In a previous work [24], the Wigner distribution function has been reconstructed from a comparable data set under the assumption that the FLASH beam is separable. Here, the formalism

(a) Reconstruction

(b) Measurement

(c) Sections $I(x,0)$ of reconstructed and measured intensity distribution
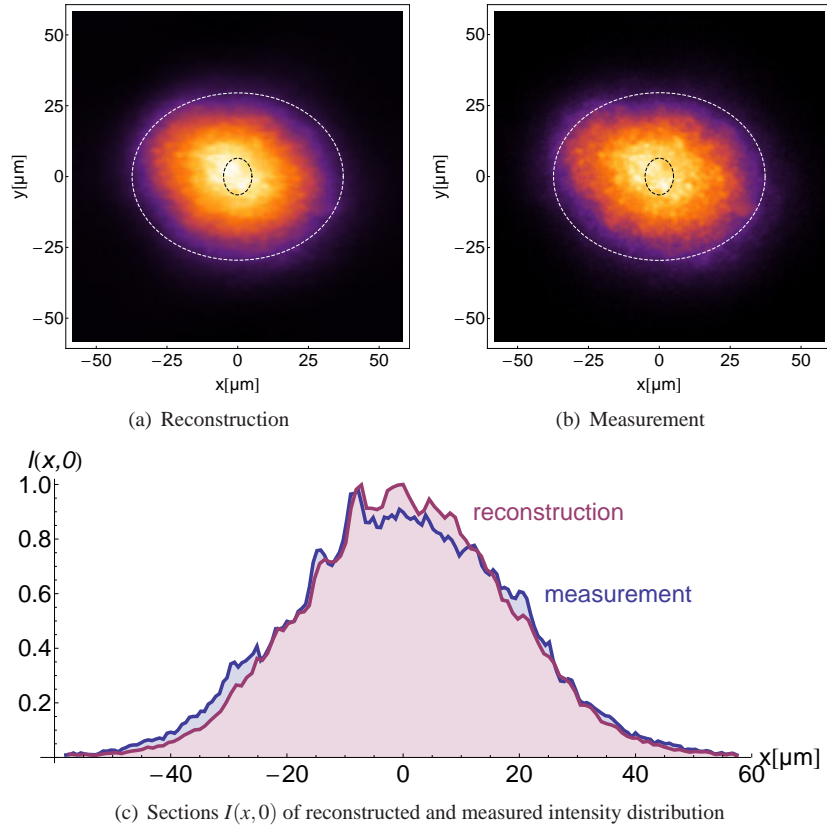
Fig. 6. Reconstructed intensity distribution $I(\vec{x}) = \int h(\vec{x}, \vec{u})\, d^2 u$ of the FLASH beam at mean waist position in (a) and corresponding measured profile in (b) ($\lambda = 24.7\,\mathrm{nm}$, $10\,\mathrm{mm}$ diameter apertures). The outer ellipse indicates the beam diameters d_x and d_y and the inner ellipse the lateral coherence lengths l_x and l_y. For better comparison, sections $I(x,0)$ are depicted in (c).

is explicitly extended to non-separable beams. However, a four-dimensional distribution is reconstructed from a three-dimensional measurement. Thus, gaps will remain in the reciprocal phase space leading to a computed Wigner distribution which possibly deviates from the true Wigner distribution. This issue is addressed by the interpolation procedure described in section 4 but cannot entirely be eliminated. Therefore, the error of the derived beam properties due to the incomplete data set should be classified.

First, for a comparison with the results derived above, the formalism that assumes a separable beam [24] is applied to the same data set. In that case, the mentioned gaps do not occur. Nonetheless, a simplification is employed that might not hold for the present beam, especially with regard to the rather complex intensity profiles in Fig. 2. The beam parameters derived by the two-dimensional calculation are summarized in Table 2 together with the values from the four-dimensional formalism. Apparently, similar results are obtained for M^2, θ and d_0. A significant deviation is found for the coherence length and the global degree of coherence. The assumption of a separable beam yields smaller values, i.e., the global degree of coherence $K_{\mathrm{sep}} = 0.020$ is $\approx 60\%$ lower than $K_{\mathrm{non-sep}} = 0.032$, derived for a non-separable beam.

Furthermore, a set of intensity profiles of a Gaussian Shell-model beam [36] is generated

to benchmark the applied procedures. For this purpose, the same wavelength, waist positions, waist diameters and divergences are used as present during the measurements at FLASH. It can be expected that this synthetic beam occupies a comparable phase space as the FEL beam and that the gaps remaining after the mapping procedure are similar. The accuracy of the algorithm is then estimated by a comparison between the computed coherence parameters and their theoretical values.

The employed intensity distribution is given by [36]

$$I(x,y,z) = \frac{I_0}{d_x(z)\,d_y(z)/(d_{0,x}\,d_{0,y})} \cdot \exp\left[\frac{-8x^2}{d_x(z)^2}\right] \cdot \exp\left[\frac{-8y^2}{d_y(z)^2}\right] \tag{10}$$

with the local beam diameter

$$d_x(z) = d_{0,x}\sqrt{1 + \left(\frac{z - z_{0,x}}{z_{R,x}}\right)^2} \tag{11}$$

and the Rayleigh length $z_{R,x} = d_{0,x}/\theta_x$ which equivalently holds for the y-direction.

$I(x,y,z)$ is evaluated with the same discretization and at the same positions as during the experiment at FLASH, resulting in 145 intensity profiles with a pixel size of $0.645\,\mu$m. From the design parameters λ, $d_{0,x}$ and θ_u, the global degree of coherence is derived by $K = K_x \cdot K_y$ with $K_x = \frac{4}{\pi} \cdot \frac{\lambda}{d_{0,x}\theta_u}$ and the coherence length by $l_x = K_x \cdot d_x$ [36].

(a) $h_x(x,u) = \int h(\vec{x},\vec{u})\,dy\,dv$ (b) $h_y(y,v) = \int h(\vec{x},\vec{u})\,dx\,du$
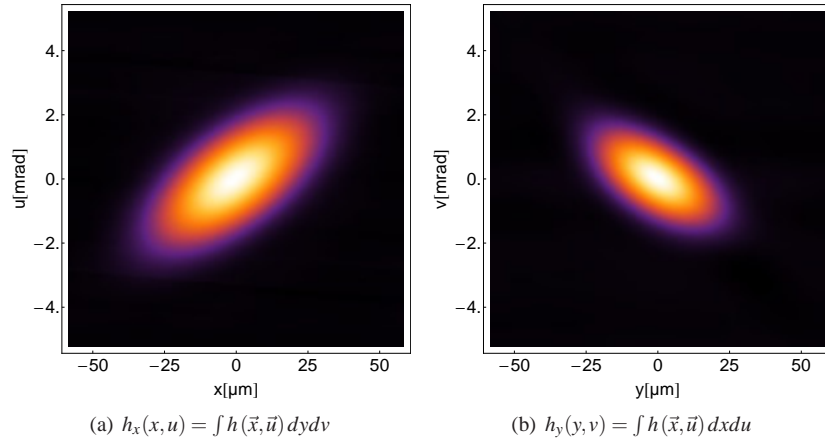
Fig. 7. Projections of the four-dimensional Wigner distribution function of the Gaussian Shell-model beam which has been simulated with design parameters corresponding to the FLASH beam.

The computed Wigner distribution function of the Gaussian Shell-model beam is depicted in terms of projections in Fig. 7. It has been derived from the simulated intensity profiles with the four-dimensional formalism, i.e., without the assumption of a separable beam. Apparently, the reconstruction does not show any artifacts. This is still the case when a noise level is included, which is comparable to the experimental data. Thus, the structures in the corresponding distribution derived for the FLASH beam shown in Fig. 3 are very likely not due to numerical errors and can be attributed to physical properties.

In Table 2 all beam parameters derived for the Gaussian Shell-model beam are summarized and both evaluation methods are compared. It is revealed that from the Wigner distribution function all predefined beam parameters can be recovered with acceptably small deviations.

For instance, both procedures result in a global degree of coherence of 0.030 which is 20% above the theoretical value of 0.025. All other beam parameters are reproduced with better accuracy.

Table 2. Comparison between both evaluation procedures, i.e., under requirement of a separable beam and without that simplification. A Gaussian Shell-model beam has been simulated with design parameters as have been derived for the FLASH beam. The computed coherence lengths $l_{x,y}$ are given in spatial units and as a fraction of the present beam diameter $d_{x,y}$ in brackets.

Beam	FLASH		Gaussian Shell-model		
Evaluation	separable	non-separable	design parameters	separable	non-separable
M_x^2	8.1	8.6	8.6	7.5	7.7
M_y^2	4.8	4.6	4.6	3.8	4.0
θ_u[mrad]	5.1	5.2	5.2	4.7	4.7
θ_v[mrad]	3.7	3.6	3.6	3.3	3.0
$d_{0,x}$[μm]	50	52	52	50	52
$d_{0,y}$[μm]	40	41	41	37	42
l_x[μm]	7.5 (0.12 d_x)	9.0 (0.13 d_x)	8.1 (0.12 d_x)	8.0 (0.13 d_x)	8.1 (0.13 d_x)
l_y[μm]	9.7 (0.18 d_y)	11.6 (0.22 d_y)	11.1 (0.22 d_y)	10.8 (0.23 d_x)	11.0 (0.24 d_y)
K	0.020	0.032	0.025	0.030	0.030

5.2. Influence of apertures

In a second set of measurements, the influence of beam divergence was studied by placing circular apertures of different sizes ranging from 10 mm down to 1 mm in diameter into the FLASH beam as described in section 3. This technique is routinely used by FLASH users to confine the photon beam to their experimental needs.

The results are summarized in Table 3. As expected [38], the coherence properties of the beam improve when employing smaller apertures. This is due to a reduction of the beam's divergence θ while its waist diameter d_0 stays more or less constant. Therefore, the Wigner distribution occupies less phase space in angular direction and, as a consequence of the well-known Fourier relations, the extent of the mutual coherence function scales up in s-direction, i.e. the coherence length l grows. Since the fraction l/d increases, also the global degree of coherence is raised.

For the smallest aperture with a diameter of 1 mm, the coherence lengths are increased by a factor of ≈ 1.6. In this case, also the waist diameters have decreased to $\approx 78\%$ of its previous value, what we attribute to the situation at a different beamline: although the FEL operating parameters were reproduced nearly as before, the beam properties might slightly differ since the beamline optic was not the same. As a benefit from both, a reduction of beam divergence and waist diameter, the global degree of coherence is increased by a factor of 6 to a value of $K = 0.198$.

6. Conclusion

From measured intensity profiles of the FLASH beam at $\lambda \approx 25$ nm with apertures of 10 mm diameter, we reconstructed the four-dimensional Wigner distribution and the entire spatial mutual

Table 3. Beam parameters of FLASH for various sizes of apertures resulting from two measurement campaigns at beamlines BL3 and BL2. The coherence lengths $l_{x,y}$ are given in spatial units and as a fraction of the present beam diameter $d_{x,y}$ in brackets.

Aperture	10 mm	5 mm	3 mm	1 mm
Beamline	3	3	3	2
λ [nm]	24.7	24.7	24.7	25.8
M_x^2	8.6	7.7	6.1	3.0
M_y^2	4.6	4.4	3.9	2.4
θ_u [mrad]	5.2	5.1	3.8	2.5
θ_v [mrad]	3.6	3.3	2.8	2.3
$d_{0,x}$ [μm]	52	48	51	38
$d_{0,y}$ [μm]	41	42	43	34
l_x [μm]	9.0 (0.13 d_x)	9.1 (0.14 d_x)	10.2 (0.17 d_x)	15.3 (0.36 d_x)
l_y [μm]	11.6 (0.22 d_y)	11.7 (0.23 d_y)	12.6 (0.26 d_y)	18.3 (0.48 d_y)
K	0.032	0.034	0.056	0.198

coherence function. Subsequently, we derived the coherence lengths to be 9.0 μm and 11.6 μm in horizontal and vertical direction, respectively. The global degree of coherence is computed to be $K = 0.032$. While the coherence lengths are in good agreement to previous studies at $\lambda = 8.0$ nm which employed Young's double pinhole experiment [14], our value for the global degree of coherence is significantly lower. Since the Wigner formalism that we applied describes an ensemble of pulses, it yields mean values for the coherence properties. In contrast, in Young's experiment only the most coherent pulses were selected for the evaluation which results in maximum values for K and $l_{x,y}$.

We also experimentally investigated the benefit on the beam properties by application of circular apertures with diameters of 10 mm down to 1 mm. Our measurements reveal that the coherence lengths can be increased to 15.3 μm and 18.3 μm in horizontal and vertical direction, respectively, when employing the smallest apertures. In that case, we find a global degree of coherence of $K = 0.198$.

Acknowledgments